

Influence of cold-wire tandem submerged arc welding parameters on weld geometry and microhardness of microalloyed pipeline steels

Mohsen Mohammadjoo¹ · Stephen Kenny^{1,2} · Laurie Collins² · Hani Henein¹ · Douglas G. Ivey^{1,*}

¹Department of Chemical and Materials Engineering, University of Alberta, Edmonton, AB, Canada T6G 1H9

²R&D Division, Evraz Inc. NA, P.O. Box 1670, Regina, SK, Canada S4P 3C7

*Corresponding author. Prof., Ph.D.; Tel.: +1 780 4922957; Fax: +1 780 4922881

E-mail address: divey@ualberta.ca (D.G. Ivey)

Abstract

Tandem submerged arc welding with an additional cold wire (CWTSAW) is being developed for pipeline manufacturing to improve productivity in terms of deposition rate and travel speed of welding. An appropriate understanding of the welding conditions to guarantee requisite weld geometry, appearance and mechanical properties is always essential in the development of a welding process. Currently, the effect of the cold-wire addition parameters on dilution and the geometry and properties of the weld metal (WM) and the heat-affected zone (HAZ) is not well understood. In this work, heat input, voltage and travel speed of both electrodes along with three main cold-wire parameters are investigated and correlated with the geometry of the weld and HAZ, i.e., aspect ratio (AR), semi-penetration ratio (SPR), reinforcement area (RA) and coarse grained heat-affected zone (CGHAZ) area, dilution and the micro-hardness of the WM and CGHAZ. The results showed that varying the cold wire parameters significantly affects the dilution, AR, SPR and micro-hardness. The addition of a cold-wire at a lagging position with a feed speed of 8.5 mm/s at 63° resulted in an overall improvement in the weld geometry, dilution and micro-hardness. Cold wire addition led to a reduction in the CGHAZ area, the amount of dilution and the micro-hardness of the CGHAZ. Microstructural analysis, using both optical microscopy and scanning electron microscopy (SEM), indicated the formation of finer prior austenite grains (PAG) and less martensite-austenite (M-A) constituent within the CGHAZ of the CWTSAW samples. The appropriate process parameters are defined to control the weld and HAZ geometry, dilution and mechanical properties.

Key words Microalloyed pipeline steel · CWTSAW · Weld and HAZ geometry · Microhardness · Dilution

1 Introduction

Submerged arc welding (SAW) has been preferred over other welding processes in pipe production due to its inherent properties, such as high deposition rate, deep penetration and capability of welding thick sections [1]. SAW uses the intense energy of the electric arc to generate the heat necessary for fusion. In the SAW process, the arc is generated between a consumable electrode and a work piece, which is shielded along with the weld puddle by a solid flux [2, 3]. To improve welding productivity in a global economy, many fabricators have resorted to tandem submerged arc welding (TSAW), which is SAW with two to five electrodes, to manufacture pipelines, pressure vessels and construction equipment [3–5]. However, in the TSAW process, heat input is increased as the number of electrodes increases because of the increase in the overall welding current and voltage for a higher deposition rate. Although TSAW provides higher productivity due to the high heat input, some adverse effects can be produced in terms of the microstructure, properties and geometry of the weld joint. The weld metal (WM) and heat-affected zone (HAZ) are particularly affected, since the weldment experiences higher peak temperatures and cools down more slowly after welding [4, 6–8].

The addition of a cold wire to the one electrode SAW process was initially proposed by Mruczek et al. in 2005 [9]. In the current research, TSAW with an additional cold-wire (CWTSAW) is developed to improve the productivity and the quality of the pipeline steel weld in terms of mechanical properties, weld geometry and dilution. The process involves two electrodes with arcs and one electrically cold electrode, which is fed at a lagging position close to the trail electrode. The authors have observed that the addition of a cold wire at the lagging position (close to the trail electrode) does not cause any reduction in the penetration depth compared with feeding a cold wire at the forward position (close to the lead electrode) which does. A cold wire at the forward position is fed into the lead electrode's arc and consumes some of the heat of the lead electrode, resulting in slightly shallower penetration, whereas a cold wire at the lagging position is fed into the tandem weld pool and/or into the trail electrode's arc with no effect on the lead electrode's arc. The cold-wire provides a higher deposition rate and better productivity for the welding process without increasing heat input compared to the TSAW process [9–11]. Furthermore, incorporating a cold-wire in TSAW moderates the heat input by consuming the energy of the trail electrode as the wire melts into the weld puddle. Accordingly, better quality welds are expected with deep penetration at lower heat inputs per mass of deposited material and with a substantial reduction in arcing time causing the formation of a smaller and shorter weld pool (compared with TSAW without a cold-wire). As such, CWTSAW technology is a promising technique for spiral welds commonly used in the pipeline industry.

From a welding process point of view, any change in the welding process parameters, such as heat input, voltage, travel speed, and polarity, and the addition of electrodes can cause considerable changes in the appearance of the weld, i.e., weld shape and geometry and HAZ geometry [12–15]. Since the microstructure and mechanical properties of the weld are significantly influenced by the composition of the WM, as well as the welding process and weld and HAZ shape and geometry [5, 16], it is essential to optimize and control the CWTSAW process parameters. On the other hand, since the operator cannot observe the weld pool in submerged arc welding as the arcs are shielded by consumable/nonconsumable granular flux, great reliance is placed on process parameter optimization [3]. The welding process optimization can be performed by the development of mathematical models through effective and strategic planning, design and execution of experiments. However, the selection of parameters and their values should be carefully done to ensure appropriate values of the process parameters. For this reason, in the current work, twenty initial welding trials were carried out prior to the designed experiments. Statistically designed experiments based on Taguchi methodology were then conducted. Accordingly, thirty-six welding runs were done and the amount of dilution, the geometry characteristics, i.e., aspect ratio (AR), semi-penetration ratio (SPR), CGHAZ area (CGHAZA) and reinforcement area (RA), and the micro-hardness of the WM and CGHAZ are measured. Three mathematical and statistical methods were employed to investigate and optimize the CWTSAW process parameters in terms of evaluating the significance of the parameters on weld and HAZ geometry, dilution and mechanical properties. The goal was to find suitable values for the welding parameters and to develop equations to predict the weld and HAZ geometry under different welding conditions. Also, the CWTSAW process was compared with the conventional TSAW process in terms of microstructural alterations and mechanical properties. Optical microscopy, scanning electron microscopy (SEM) and micro-hardness measurements were utilized to correlate the microstructures with property changes in the CGHAZ.

2 Experimental Procedure

2.1 Microalloyed steel and procedure of CWTSAW

Weld samples were prepared by CWTSAW of 13.4 mm thick plates of X70 microalloyed steel. A 90° V-shaped bevel with 5 mm depth was machined in the steel plates prior to welding. Direct current electrode positive (DCEP) and square wave alternating current (ACSQ) polarity were employed using constant current type power sources to operate the lead and trail electrodes, respectively. The cold-wire composition was the same as the electrodes. The compositions of the microalloyed steel and the consumable electrodes are indicated in Table 1.

The 4 mm diameter wires for the electrodes and cold-wire were selected based on EN756/EN14295 (BA-S2Mo, Bavaria, Germany) and AWS A5.17/A5.23 (EA2). The consumable flux was chosen according to EN 760 (BF6.5, Bavaria, Germany).

The CWTSAW process setup and the fixed welding parameters are illustrated in Fig. 1. Eight welding parameters including five main welding parameters, i.e., heat-input and voltage of the lead and trail electrodes and travel speed, and the three main cold-wire parameters, i.e., position, angle and feed speed, were varied through welding (Table 2). According to the eight welding parameters with mixed levels (a combination of two and three levels) considered in this work, an L36 orthogonal array, Taguchi methodology [17] was used and thirty-six welding runs were conducted to investigate the correlation of CWTSAW parameters with the weld and HAZ geometry, dilution and mechanical properties.

The geometry characteristics (i.e., SPR, AR, RA and CGHAZA), dilution and micro-hardness values were measured using a stereomicroscope (Fisher Scientific, Canada) and Vickers micro-hardness machine (Wilson VH3100, Buehler, Germany), respectively. Three measurements were carried out for each welding run to increase the accuracy of the final data for process analysis. Accordingly, 108 specimens were cut at the transverse direction relative to the welding direction and then mounted and polished according to ASTM E3-11 standard [18]. The weld samples were macro-etched with 4% Nital to reveal the WM, HAZ and their boundaries (Fig. 2b).

2.1.1 Initial trials for welding parameter selection

In TSAW, the lead electrode is positioned to generate sufficient penetration depth of the weld and the trail electrode provides filling of the bevel, resulting in adequate joining of the metal pieces of interest. Accordingly, DCEP and ACSQ polarities were selected for the lead and trail electrode, respectively, as DCEP on the lead electrode causes deeper penetration and ACSQ on the trail electrode provides increased deposition rate relative to DCEP polarity [19]. Prior to starting the designed experiments, twenty welding trial runs were conducted to generate an overview of the CWTSAW process. During the early stages of setting up the CWTSAW process, the distance between the trail electrode and the cold-wire was considered as a variable; however, through welding trials it was determined that the melting rate of the cold-wire increased as the cold-wire/trail electrode separation distance was decreased. In addition, the shape and size of weld bead changed when the cold wire position and angle were varied. Therefore, the position, angle and feed rate of the cold-wire were used as the main cold-wire parameters. Stick-out and electrode distance were set at 13 and 18 mm, respectively. The

extreme values of the parameters, in particular those for the cold-wire, were examined through welding trials by visual inspection of the bead for visible defects, such as surface porosity, burn-through and undercutting. In many previous research studies, current has been selected as a welding variable; however, it was decided not to include current as a variable. Since running a welding system at high current and low travel speed and vice versa is not a reasonable endeavour, in this research work heat input was considered as a major parameter and the current was set during welding according to the voltage and travel speed for welding in each run. The current is calculated according to Equation 1:

$$HI \left(\frac{kJ}{mm} \right) = \frac{\mu \cdot (V \cdot I)}{1000 \cdot TS} \quad (1)$$

where μ is the arc efficiency, which depends on the welding process, and HI , V , I and TS are the heat input, voltage, current and travel speed (mm/s), respectively. The arc efficiency for submerged arc welding is 0.9-1.0.

2.2 Developing the Experimental Design Matrix

Since the results and conclusions that can be drawn from the experiment depend to a large extent on the manner in which the data are collected, a well-designed experiment is of major importance. Experimental design methods were originally developed by Fisher [20, 21]. However, classical experimental design methods are too complex and are not easy to use. Furthermore, a large number of experiments have to be carried out as the number of the process parameters increases [22, 23]. The Taguchi method developed by Genichi Taguchi employs a design of orthogonal arrays to study the entire parameters with a small number of experiments relative to other experimental design methods. It was proposed that engineering optimization of a process or product should be carried out in a three-step approach: system design, parameter design and tolerance design [17, 24]. The objective of parameter design is to optimize the settings of the process parameter values for improving quality characteristics and to identify optimal process parameter values. In addition, it is expected that the optimal process parameter values obtained from parameter design will be insensitive to variation in environmental conditions and other noise factors. The quality engineering method of Taguchi methodology, i.e., employing designed experiments, provides an efficient and systematic way to optimize designs for performance, quality and cost. The use of Taguchi methodology simplifies the optimization procedure for determining optimal welding parameters in the SAW process. Dhas et al. [22], Tarng et al. [14, 23] and Yang [25, 26] have studied the optimization of SAW process parameters using Taguchi methodology.

According to the orthogonal arrays proposed by Taguchi, the design matrix for the welding process, including five parameters with two levels and three parameters with three levels, is an L36 orthogonal array which comprises 36 weld runs in which the levels for each parameter are equally repeated through the design. The designed experiments based on the L36 orthogonal array are summarized in Table 3.

3 Results and Discussion

The geometry characteristics, dilution and micro-hardness were measured to correlate the weld parameters with the weld characteristics and properties. More details regarding the measured characteristics are provided in the Appendix (Table A.1). SPR and AR are unitless characteristics defined by Equations 2 and 3, respectively.

$$AR = \frac{\text{Penetration Depth}}{\text{Bead Width}} \quad (2)$$

$$SPR = \frac{\text{Bead Width}}{\text{weld width at half of penetration}} \quad (3)$$

Since the amount of dilution will influence the composition of the weld pool, and influence its metallurgical and mechanical properties, it is important to optimize the welding process based on the weld dilution. Dilution was calculated using the expression reported by Lancaster in Equation 4 [27]:

$$Dilution = \frac{\text{weight of parent metal melted}}{\text{total weight of fused metal}} = \frac{(\text{Penetration area} - \text{bevel area})}{(\text{penetration area} + \text{reinforcement area})} \quad (4)$$

where penetration depth, bead width and weld width at half penetration are indicated in Fig. 2. As stated earlier, process optimization was carried out according to dilution and weld and HAZ geometry. Fig. 2 depicts a macrograph of an X70 microalloyed steel welded by CWTSAW showing the weld geometry characteristics.

3.1 CWTSAW Process Parameters Investigation

Three analysis steps were performed on the weld characteristic data to investigate and optimize the CWTSAW process parameters. The first step was to understand the significance of the welding parameters on the geometry characteristics and dilution; this was done by the analysis of variance (ANOVA) method. Taguchi methodology augmented the optimization procedure by evaluating the parameter levels resulting in the optimal effect on geometry characteristics and dilution. Since there is a need in welding related industries to be able to predict weld geometry for different combinations of welding parameters, three-order multiple regression analysis (TOMRA) was employed to develop equations predicting geometry characteristics and dilution. Minitab software 17.0, a commercial statistical package, was utilized to perform the mathematical data analysis.

ANOVA was carried out on the data extracted from geometry, dilution and micro-hardness measurements. The purpose of ANOVA was to determine which welding process parameters significantly affected the parametric characteristics (i.e., geometry, dilution and micro-hardness) when all eight parameters were varied. The significance of the welding parameters on the parametric characteristics was mainly evaluated in terms of the F-test [28], P-value [13, 22, 25, 26] and percentage contribution of each parameter. The detailed raw data extracted from ANOVA for the sum of the squares (adj SS), F-values and P-values of the welding variables are presented in the Appendix (Table A.2). P-value is the probability of significance. A 90% confidence level was selected in the data analysis, which means that if the P-value for a factor is less than 0.1 then the welding parameter significantly influences the parametric characteristic. The F-test represents the systematic variance; if the independent variable (welding parameter) has an effect, then the dependent variable (parametric characteristic) should vary under different experimental conditions. Therefore, a higher F-value for a variable indicates that the parameter has a significant effect on the parametric characteristic [29]. As an example, the parameters which are highly significant for SPR are trail electrode voltage, travel speed and cold-wire feed speed.

The percentage contribution of the parameters was calculated by measuring the sum of the squared deviations (deviations from the total mean value) and converting into contributions for each of the process parameters, according to Equation 5:

$$\text{Percentage contribution: } \rho\% = \frac{SS_i}{SS_{tot.}} \quad (5)$$

where ρ is the contribution in percent of each parameter to the performance characteristic and SS_i and $SS_{tot.}$ are the sum of the squares for each parameter and the total sum of the squares, respectively. The percentage contribution for each of the process parameters in the total sum of the squared deviations can be used to evaluate the importance of the process parameter change on the performance characteristic. Based on Equation 5, the percentage contribution for each welding parameter was calculated and the values are shown in Fig. 3. Accordingly, the maximum percentage contribution for the cold-wire parameters (CWP, CWA and CWFS) on the geometry characteristics was 32.6% for AR. Also, the contribution for dilution variation was 35.7%. However, the other welding parameters (i.e., heat-input, voltage and TS) had a greater effect on the geometry characteristics and dilution of the weld compared with the cold-wire parameters.

Micro-hardness measurements of thirty-six weld samples were done along the BM, HAZ and WM according to ASTM E384 [30] to investigate the significance of CWTSAW parameters on the mechanical

properties of the WM and CGHAZ. A 500 g load was applied for a dwell time of 14 s per indentation. In total, 40 test points were examined per weld sample, with an average of 10-12 indents across each of the CGHAZ and WM. Fig. 4 depicts the hardness measurement mapping for a typical welded sample using CWTSAW.

According to the ANOVA results for the hardness measurements, cold-wire parameters i.e., position, angle and feed speed of the cold-wire, show a significant effect on the hardness of the WM and CGHAZ. Other welding parameters, for the ranges studied, did not have a significant effect on the hardness for either the WM or CGHAZ. It should be noted that the parameter ranges were selected based on initial welding trials. Microstructural analysis was carried out on two weld samples and is discussed in the next section. As stated earlier, the percentage contribution for each of the process parameters can also be used to evaluate the importance of a process parameter change on the performance characteristic. As shown in Fig. 3, TS and the cold-wire parameters, in particular variation in CWFS, show a significant contribution to the variation in hardness of the WM and CGHAZ compared with the other welding parameters. The CWFS effect is related to the heat introduced to the weldment and, consequently, the cooling rate within the WM and CGHAZ.

The control factors that may contribute to reducing variation (improving quality) can be quickly identified by looking at the amount of variation present as a response. The signal-to-noise ratio (S/N) was used to determine the deviation of the geometry characteristic and dilution from the desired value. Dilution, RA and CGHAZA belong to a “lower-the-better” quality characteristic. SPR and AR are “higher-the-better” quality characteristics. Since there is no general agreement to judge and determine whether lower or higher hardness leads to better overall mechanical properties, S/N ratio analysis was not performed on the micro-hardness values. The S/N ratio can be expressed as Equations 6 and 7 [17, 24]:

$$\text{Lower-the-better: } (S/N)_{ratio} = -10 \log_{10} \left(\frac{1}{n} \sum_{i=1}^n y_{ij}^2 \right) \quad (6)$$

$$\text{Higher-the-better: } (S/N)_{ratio} = -10 \log_{10} \left(\frac{1}{n} \sum_{i=1}^n \frac{1}{y_{ij}^2} \right) \quad (7)$$

where y_{ij} and n are the experimental values of the i th performance characteristic in the j th experiment and the number of trials, respectively. A level of input parameter with a higher average S/N ratio is considered as the best value of the parameter with an optimal effect on the geometry characteristics, i.e., SPR, AR, CGHAZA and RA, and dilution, since the largest S/N ratio indicates that the signal obtained from the considered parameters is much higher than the random effects of the noise factors [17, 24]. The average S/N ratios for dilution and the geometry characteristics are provided in the Appendix (Table A.3). The higher S/N ratio for each parameter level shows an optimal effect on the parametric characteristics. Based on the calculated S/N ratio of the welding

parameters, the suitable levels for the CWTSAW process parameters are indicated in Table 5. Overall, it can be concluded that the optimal parametric characteristics (i.e., weld and HAZ geometry and dilution) are achieved when the cold-wire is fed at a lagging position (level 1) with a feed speed of 8.5 mm/s (level 1) and a high angle of 63° (level 3).

Multiple regression analysis, a statistical tool to ascertain the relationships among variables, was employed to predict the geometry characteristics of the welds prepared by the CWTSAW process. The developed empirical equations predict the weld geometry for different combinations of the CWTSAW parameters, which is important from an engineering and industrial perspective. The most frequently used method is that of linear equations. Three-order multiple regression analysis (TOMRA) considers the interaction of variables and their contributions to predicting the characteristics. TOMRA takes the form shown in Equation 8:

$$Y = \alpha_0 + \sum_{i=1}^8 (\alpha_i \cdot x_i) + \sum_{i=1}^8 (\alpha_{ii} \cdot x_i^2) + \sum_{i=1}^8 \sum_{j>i}^8 (\alpha_{ij} \cdot x_i \cdot x_j) + \sum_{i=1}^8 (\alpha_{iii} \cdot x_i^3) + \sum_{i=1}^8 \sum_{j>i}^8 \sum_{k>j}^8 (\alpha_{ijk} \cdot x_i \cdot x_j \cdot x_k) \quad (8)$$

where Y is the dependent variable (geometry characteristics) which is to be predicted and x_i is the known variables (welding parameters) on which the predictions are made; α , α_i , α_{ii} , α_{ij} , α_{iii} and α_{ijk} are the coefficients. Multiple regression analysis of the CWTSAW process parameters is expressed in third-order equations, which are presented in the Appendix.

TOMRA employs the same analysis strategy as the ANOVA in which parameter interaction is accounted for as well. The welding parameters (including interactions) which result in higher sum of the squares (deviation from the mean value of a parametric characteristic) are considered to predict the parametric characteristic. As an example, only 19 variables from a total of 92 possible variables (including parameter interactions) are considered in the SPR equation, resulting in an equation which fits the observed values. Accordingly, the computed values for the geometry characteristics were compared with the observed values from the experiments and showed good fitting. The validity of the equations was tested with four random combinations of weld and cold-wire parameters (Table 6). The geometry characteristics of four welds with different CWTSAW parameter levels were measured and compared with the calculated values from the equations and showed good correlation with the actual values (Fig. 5).

3.2 CWTSAW and TSAW Comparison

Two weld samples, prepared by the CWTSAW and TSAW processes, were evaluated in terms of weld geometry, dilution and the CGHAZ micro-hardness. The welding conditions for preparation of the two weld

samples are indicated in Table 4. Fig. 6 depicts macrographs of the two weld samples, both with the same heat input of 2.15 kJ/mm. A comparison of the welds prepared by CWTSAW and conventional TSAW is given in Table 7. There is a significant reduction from 21.3 to 19.1 mm² and 0.65 to 0.56 in the CGHAZA and dilution, respectively. Also, the micro-hardness of the CGHAZ was reduced by addition of a cold-wire to the TSAW process. It is generally accepted that the part of the HAZ adjacent to the fusion line, which is characterized by the coarse grains associated with the M-A constituents, localized brittle zones (LBZ), is the weakest region resulting in low toughness. The cold-wire addition showed a reduction in the size of CGHAZ and a reduction in the CGHAZ micro-hardness, due to a reduction in the actual heat introduced to the weldment and the corresponding microstructural changes.

SEM and optical metallography of the CGHAZ of the steel samples, welded by both welding processes, indicate that the prior austenite grain (PAG) size decreased as the cold-wire was added to the welding process. The PAG size of the CGHAZ (0-300 μm away from the fusion line) decreased from 56 to 45 μm on adding the cold-wire. This phenomenon is attributed to a reduction in the actual heat introduced to the weldment, lowering of the peak temperature, reduction in the retention time in the austenitization temperature range (1100-1400°C) and an increase in the cooling rate by adding the cold-wire. Eight SEM and optical micrographs were analyzed from the CGHAZ of each weld sample at the transverse direction relative to the welding direction. Fig. 7 shows the microstructure of the CGHAZ for the CWTSAW and TSAW samples. The CGHAZ microstructure of the TSAW sample (higher heat input) is comprised of large PAGs, polygonal ferrite and large elongated M-A constituents along the PAG boundaries. In contrast, the CGHAZ microstructure of the CWTSAW sample (lower heat input) has smaller PAGs and a region of polygonal ferrite associated with blocky shaped M-A constituents.

The M-A constituents appear as shiny white phase using LePera's etchant [31] (Fig. 7d and 7h). The M-A fraction in the CGHAZ of each weld sample was analyzed using ImageJ software (Fig. 7j-n). Both optical and SEM micrographs were used for the M-A fraction analysis. The M-A fraction in the CGHAZ of the TSAW and CWTSAW samples, calculated from the SEM micrographs (Fig. 7n and 7m), was 7.6% and 5.4%, respectively, indicating a reduction in the fraction of M-A as a consequence of PAG size reduction [32–35] by cold-wire addition. The M-A fraction in the CGHAZ calculated from the optical micrographs (Fig. 7j and 7i), was 5.8% and 3.9% for the TSAW and CWTSAW samples, respectively. The trend is the same and the quantitative values are quite similar for both techniques, which confirm the validity of the M-A identification in the SEM images. The larger M-A constituents in the CGHAZ of the TSAW sample are due to the higher martensite start temperature (Ms) for samples with larger PAGs [33, 34, 36, 37]. Bhadeshia et al. [34, 38] found that as the PAG

size decreases the Ms temperature also decreases, resulting in a lower volume fraction of martensite. The fraction of martensite is a function of the undercooling below the Ms temperature according to the classical Koistinen-Marburger (KM) equation [32] and the geometrical partitioning model by Fisher et al. [39]. According to the proposed models, the martensite volume fraction formed in the early stages of the transformation is proportional to the cube of the PAG size; hence, “the fraction of the transformation needed to detect Ms is reached at a smaller undercooling when the PAG size is larger” [34]. Therefore, a coarser PAG size increases the fraction and size of the M-A constituent. Li et al. [33] and Yu et al. [35] showed that a coarse PAG size associated with a coarse M-A constituent is the dominant factor in promoting brittle fracture in the CGHAZ. Accordingly, there is a concurrent effect of both grain size refinement and M-A transformation, which plays a significant role in the strength, hardness and toughness of the HAZ. Due to the formation of the M-A constituent, there is a higher proportion of localized hardened zones in the CGHAZ of the TSAW sample compared with the CWTSAW sample. This shows up as higher micro-hardness values in the CGHAZ for the TSAW sample relative to the CWTSAW sample. Also, M-A constituents (LBZs) did not form along PAG boundaries in the HAZ of the CWTSAW sample, which should result in improved fracture toughness for the HAZ.

4 Conclusions

The influence of the Cold-wire tandem submerged arc welding (CWTSAW) process parameters on the geometry, dilution and micro-hardness of the weld and the HAZ was investigated and optimized for the first time in this research work. The following conclusions were drawn from the research work done on CWTSAW:

- 1) Variations in the cold-wire parameters showed significant effects on the geometry characteristics, i.e., semi-penetration ratio (SPR) and aspect ratio (AR), dilution and the weld metal (WM) and coarse grain heat affected zone (CGHAZ) micro-hardness. The effects are a consequence of the considerable reduction in the total heat introduced to the weldment and the subsequent change in cooling rate when a cold-wire is added to the molten pool during CWTSAW.
- 2) The maximum effect of cold-wire parameter variation on geometry characteristics and dilution was 33.1% and 39.5%, respectively, compared with other parameters. The addition of cold-wire at a lagging position with a feed speed of 8.5 mm/s at 63° resulted in an overall improvement in the weld geometry and properties.

- 3) There was a 14.0% and 10.3% reduction in dilution and the CGHAZ area, respectively, for the CWTSAW process, because of a reduction in the overall heat introduced to the weldment.
- 4) Microstructural analysis, using both optical microscopy and scanning electron microscopy (SEM), indicated the formation of finer prior austenite grains (PAG) and less M-A constituent within the CGHAZ of the CWTSAW samples, which is attributed to lower actual heat introduced to the weldment and faster cooling rates. These effects also led to lower micro-hardness values in the CGHAZ of the CWTSAW samples.

Acknowledgements

The authors are grateful to the Natural Sciences and Engineering Research Council (NSERC) of Canada and to the following companies for providing research funding: Evraz Inc. NA, TransCanada PipeLines Ltd., Enbridge Pipelines Inc., UT quality Inc. and Alliance Pipeline Ltd. Special thanks go to the Research and Development Division of Evraz Inc. NA for providing equipment and technical assistance to conduct the welding runs.

Appendix

The measured values for SPR, AR, CGHAZA, RA, Dilution, WM and CGHAZ micro-hardness are presented in Tables A.1 and A.2 in this section. The S/N ratios for the welding parameters for each parametric characteristic are indicated in Table A.3.

The developed empirical equations to predict the weld and HAZ geometry, performed by the TOMRA method, are presented below:

$$SPR = 33.3 - 16.4 \cdot C - 0.56 \cdot D - 0.92 \cdot E - 0.18 \cdot F - 0.23 \cdot G - 0.8 \cdot H + 0.56 \cdot C \cdot E + 0.49 \cdot C \cdot G - 0.6 \cdot C \cdot H + 0.01 \cdot D \cdot E + 0.01 \cdot D \cdot F - 0.01 \cdot D \cdot G + 0.06 \cdot D \cdot H + 0.01 \cdot E \cdot G + 0.03 \cdot E \cdot H - 0.02 \cdot C \cdot E \cdot G + 0.01 \cdot C \cdot E \cdot H + 0.0003 \cdot D \cdot E \cdot G - 0.0017 \cdot D \cdot E \cdot H$$

$$AR = 3199.7 - 110.4 \cdot A - 818 \cdot B - 543.3 \cdot C - 35.61 \cdot D - 17.95 \cdot E - 136.9 \cdot F + 11.12 \cdot G - 2.39 \cdot H + 32.82 \cdot A \cdot B + 2.26 \cdot A \cdot C + 3.13 \cdot A \cdot F + 0.07 \cdot A \cdot G + 1.81 \cdot A \cdot H + 0.67 \cdot B \cdot D + 32.22 \cdot B \cdot F - 2.09 \cdot B \cdot G + 3.23 \cdot B \cdot H + 23.55 \cdot C \cdot F - 1.87 \cdot C \cdot G + 1.55 \cdot D \cdot F - 0.13 \cdot D \cdot G - 0.03 \cdot D \cdot H + 0.79 \cdot E \cdot F - 0.07 \cdot E \cdot G - 0.01 \cdot F \cdot G - 0.006 \cdot G \cdot H - 0.28 \cdot A \cdot B \cdot G - 1.65 \cdot A \cdot B \cdot H$$

$$CGHAZA = 154 + 2.36 \cdot D - 17.8 \cdot F - 43.7 \cdot A \cdot C + 7 \cdot B \cdot F + 0.25 \cdot D \cdot F + 0.08 \cdot D \cdot G - 67 \cdot A \cdot B^2 + 77.4 \cdot A \cdot B \cdot C + 2.27 \cdot A \cdot B \cdot D + 1.69 \cdot A \cdot B \cdot F - 1.91 \cdot A \cdot C \cdot D - 0.03 \cdot A \cdot D \cdot G - 0.01 \cdot A \cdot F^2 + 0.01 \cdot A \cdot G^2 - 0.01 \cdot A \cdot G \cdot H - 69.3 \cdot B^2 \cdot C + 57 \cdot B \cdot C^2 - 0.14 \cdot B \cdot D^2 - 0.01 \cdot B \cdot F \cdot G - 0.04 \cdot C \cdot G \cdot H - 0.002 \cdot D \cdot F \cdot G - 0.0004 \cdot E \cdot G^2 + 0.002 \cdot E \cdot G \cdot H + 0.001 \cdot F^2 \cdot G$$

$$RA = 276 - 270 \cdot B - 159 \cdot C - 1.14 \cdot A \cdot H + 149 \cdot B \cdot C + 3.13 \cdot A \cdot B \cdot H + 0.79 \cdot A \cdot C \cdot H - 0.11 \cdot A \cdot D \cdot H + 1.34 \cdot B^2 \cdot D - 0.0003 \cdot D^2 \cdot E$$

Note that the parameters A, B, C, ... correspond to the symbols given in the first column of Table 2.

References

1. Qiao GY, Xiao FR, Zhang XB, et al. (2009) Effects of contents of Nb and C on hot deformation behaviors of high

- Nb X80 pipeline steels. *Trans Nonferrous Met Soc China (English Ed)* 19:1395–1399. doi: 10.1016/S1003-6326(09)60039-X
2. Nugent, RM, Dybas, RJ, Hunt, JF, Meyer D (2009) *Submerged Arc Welding*. AWS Welding Handbook, 8th edn. Am. Weld. Soc., Miami
 3. ESAB (2013) *Submerged Arc Welding (Technical Handbook)* 1–94
 4. Kiran D V, Alam SA, De A (2013) Development of process maps in two-wire tandem submerged arc welding process of HSLA steel. *J Mater Eng Perform* 22:988–994. doi: 10.1007/s11665-012-0381-2
 5. Moeinifar S, Kokabi AH, Hosseini HRM (2011) Role of tandem submerged arc welding thermal cycles on properties of the heat affected zone in X80 microalloyed pipe line steel. *J Mater Process Technol* 211:368–375. doi: 10.1016/j.jmatprotec.2010.10.011
 6. Beidokhti B, Kokabi AH, Dolati A (2014) A comprehensive study on the microstructure of high strength low alloy pipeline welds. *J Alloys Compd* 597:142–147. doi: 10.1016/j.jallcom.2014.01.212
 7. Farhat H (2007) Effects of multiple wires and welding speed on the microstructures and properties of submerged arc welded X80 steel. PhD Dissertation, University of Saskatchewan
 8. Murugan N, Gunaraj V (2005) Prediction and control of weld bead geometry and shape relationships in submerged arc welding of pipes. *J Mater Process Technol* 168:478–487. doi: 10.1016/j.jmatprotec.2005.03.001
 9. Mruczek MF, Konkol PJ (2005) Twin-arc and cold-wire-feed submerged-arc welding of HSLA-100 steel. *Conf. Proceedings, Am. Weld. Soc*
 10. Ramakrishnan M, Muthupandi V (2012) Application of submerged arc welding technology with cold wire addition for drum shell long seam butt welds of pressure vessel components. *Int J Adv Manuf Technol* 1–12. doi: 10.1007/s00170-012-4230-0
 11. Ramakrishnan M, Padmanaban K, Muthupandi V (2013) Studies on fracture toughness of cold wire addition in narrow groove submerged arc welding process. *Int J Adv Manuf Technol* 68:293–316. doi: 10.1007/s00170-013-4729-z
 12. Akkas N, Karayel D, Ozkan SS, et al. (2013) Modeling and analysis of the weld bead geometry in submerged arc welding by using adaptive neurofuzzy inference system. *Math Probl Eng*. doi: 10.1155/2013/473495
 13. Benyounis KY, Olabi AG (2008) Optimization of different welding processes using statistical and numerical approaches - A reference guide. *Adv Eng Softw* 39:483–496. doi: 10.1016/j.advengsoft.2007.03.012
 14. Targ YS, Yang WH (1998) Application of the Taguchi Method to the Optimization of the Submerged Arc Welding Process. *Mater Manuf Process* 13:455–467. doi: 10.1080/10426919808935262
 15. Shen S, Oguocha INA, Yannacopoulos S (2012) Effect of heat input on weld bead geometry of submerged arc welded ASTM A709 Grade 50 steel joints. *J Mater Process Technol* 212:286–294. doi: 10.1016/j.jmatprotec.2011.09.013
 16. Connor LP, O'Brien RL (1987) *Welding Handbook: Welding Technology*. Am. Weld. Soc

17. Taguchi G, Rafanelli AJ (1994) Taguchi on Robust Technology Development: Bringing Quality Engineering Upstream. *J Electron Packag* 116:161. doi: 10.1115/1.2905506
18. ASTM (2011) E3-11 Standard Guide for Preparation of Metallographic Specimens 1. ASTM Copyright i:1–12. doi: 10.1520/E0003-11.2
19. Pepin J, Penniston C, Henein H, et al. (2012) Using semipenetration ratio to characterise effects of waveform variables on bead profile and heat affected zone with single electrode submerged arc welding. *Can Metall Q* 51:284–293. doi: 10.1179/1879139512Y.0000000018
20. Fisher RA (1956) Statistical methods for research workers. *Q J R Meteorol Soc* 82:119–119. doi: 10.1002/qj.49708235130
21. Montgomery DC (2009) *Design and Analysis of Experiments*, 7th edn. Wiley, New York
22. Dhas JER, Kumanan S (2011) Optimization of parameters of submerged arc weld using non conventional techniques. *Appl Soft Comput J* 11:5198–5204. doi: 10.1016/j.asoc.2011.05.041
23. Tarng YSS, Juang SCC, Chang CHH (2002) The use of grey-based Taguchi methods to determine submerged arc welding process parameters in hardfacing. *J Mater Process Technol* 128:1–6. doi: 10.1016/S0924-0136(01)01261-4
24. Roy R (1990) *A primer on the taguchi method*. Van Nostrand Reinhold, New York
25. Yang LJ, Chandel RS, Bibby MJ (1993) An analysis of curvilinear regression equations for modeling the submerged-arc welding process. *J Mater Process Tech* 37:601–611. doi: 10.1016/0924-0136(93)90121-L
26. Yang LJ, Chandel RS, Bibby MJ (1992) The effects of process variables on the bead width of submerged-arc weld deposits. *J Mater Process Tech* 29:133–144. doi: 10.1016/0924-0136(92)90430-Z
27. Kou S (2003) *Welding Metallurgy*, 2nd edn. Wiley, New York. doi: 10.1016/j.theochem.2007.07.017
28. Fisher SRA (1971) *The Design of Experiments*. Hafner Publ Co, New York 1–27
29. Arnold SF (2006) *Design of Experiments with MINITAB*. *Am Stat*. doi: 10.1198/tas.2006.s46
30. ASTM (2012) E384-11: Standard Test Method for Knoop and Vickers Hardness of Materials. *ASTM Stand* 1–43. doi: 10.1520/E0384-11E01.2
31. LePera FS (1979) Improved etching technique for the determination of percent martensite in high-strength dual-phase steels. *Metallography* 12:263–268. doi: 10.1016/0026-0800(79)90041-7
32. Koistinen DP, Marburger RE (1959) A general equation prescribing the extent of the austenite-martensite transformation in pure iron-carbon alloys and plain carbon steels. *Acta Metall* 7:59–60. doi: 10.1016/0001-6160(59)90170-1
33. Li X, Ma X, Subramanian S V., et al. (2014) Influence of prior austenite grain size on martensite-austenite constituent and toughness in the heat affected zone of 700MPa high strength linepipe steel. *Mater Sci Eng A* 616:141–147. doi: 10.1016/j.msea.2014.07.100
34. Yang HS, Bhadeshia HKDH (2009) Austenite grain size and the martensite-start temperature. *Scr Mater* 60:493–495. doi: 10.1016/j.scriptamat.2008.11.043

35. Yu L, Wang HH, Hou TP, et al. (2014) Characteristic of martensite–austenite constituents in coarse grained heat affected zone of HSLA steel with varying Al contents. *Sci Technol Weld Join* 19:708–714. doi: 10.1179/1362171814Y.0000000246
36. Heinze C, Pittner A, Rethmeier M, Babu SS (2013) Dependency of martensite start temperature on prior austenite grain size and its influence on welding-induced residual stresses. *Comput Mater Sci* 69:251–260. doi: 10.1016/j.commatsci.2012.11.058
37. Prawoto Y, Jasmawati N, Sumeru K (2012) Effect of Prior Austenite Grain Size on the Morphology and Mechanical Properties of Martensite in Medium Carbon Steel. *J Mater Sci Technol* 28:461–466. doi: 10.1016/S1005-0302(12)60083-8
38. Bhadeshia HKDH (2013) About calculating the characteristics of the martensite-austenite constituent. *Proc Int Semin Weld High Strength Pipeline Steels, CBMM TMS* 99–106
39. Fisher JC, Hollomon JH, Turnbull D (1949) Kinetics of the austenite-martensite transformation. *Trans Am Inst Min Metall Eng* 185:691–700

Figure Captions:

Fig. 1 CWTSAW process setup. a) Schematic view of fixed welding variables and weldment geometry. b) Actual welding setup

Fig. 2 (a) Schematic of the welded steel indicating different weld zones. (b) Optical macrograph of X70 microalloyed steel welded by CWTSAW, indicating the geometry characteristics

Fig. 3 Significance of CWTSAW process parameters on geometry characteristics, dilution and micro-hardness of the WM and the CGHAZ. The colour scheme is the same for all performance characteristics

Fig. 4 Micro-hardness mapping along the BM, HAZ and WM of a typical weld prepared by CWTSAW. The micrograph in the inset shows an indentation in the CGHAZ

Fig. 5 Comparison of calculated values and observed values for (a) SPR, (b) AR, (c) CGHAZA and (d) RA. The confirmatory test results are superimposed on the graphs (triangles). The straight line indicates the ideal condition in which the predicted values are equal to the observed values

Fig. 6 Macrographs of welds produced by: a) CWTSAW and b) TSAW. There is a reduction of ~10% in the CGHAZ area for the CWTSAW sample relative to the TSAW sample. The CGHAZ has been outlined in both images

Fig. 7 SEM SE images (a,b,e,f) and optical micrographs (c,d,g,h) of the CGHAZ of the steel welded using CWTSAW (a-d) and TSAW (e-h). M-A constituent analysis in the CGHAZ of the CWTSAW and TSAW sample (j,m) and the CGHAZ of the TSAW sample (k,n). Some of the PAGs are outlined in (c) and (g)

Figures:

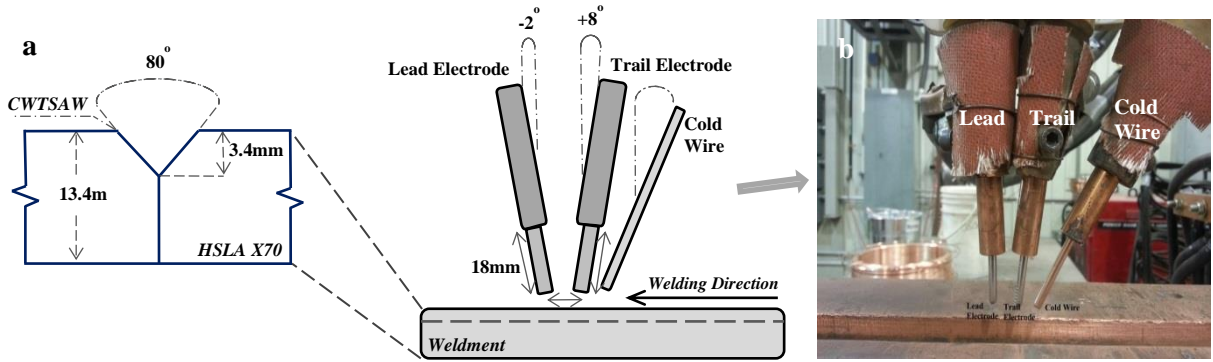


Fig. 1

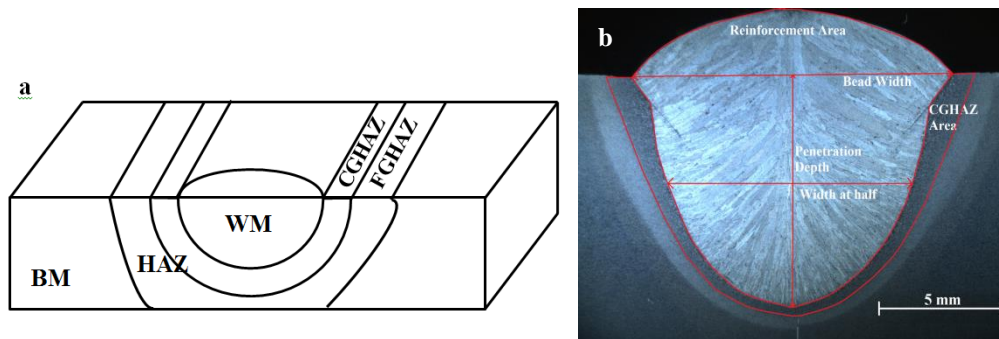


Fig. 2

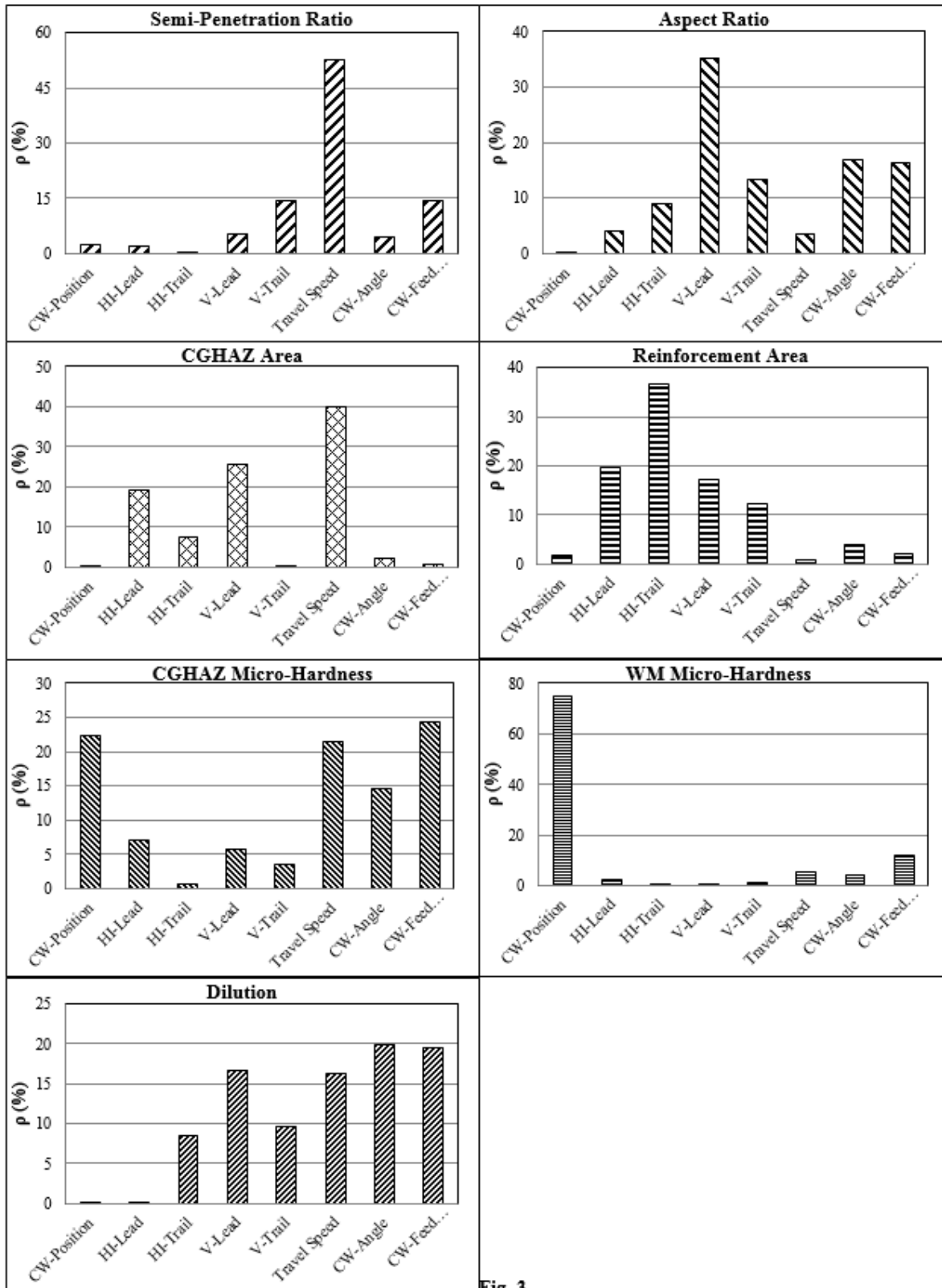


Fig. 3

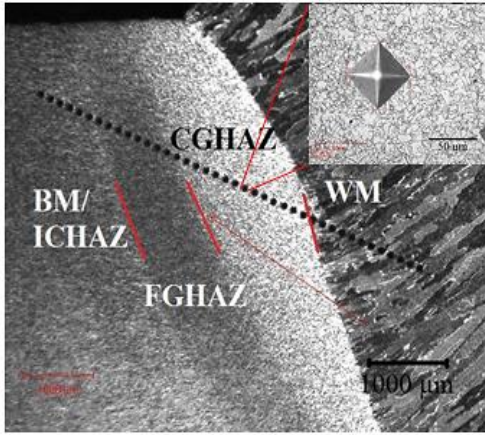


Fig. 4

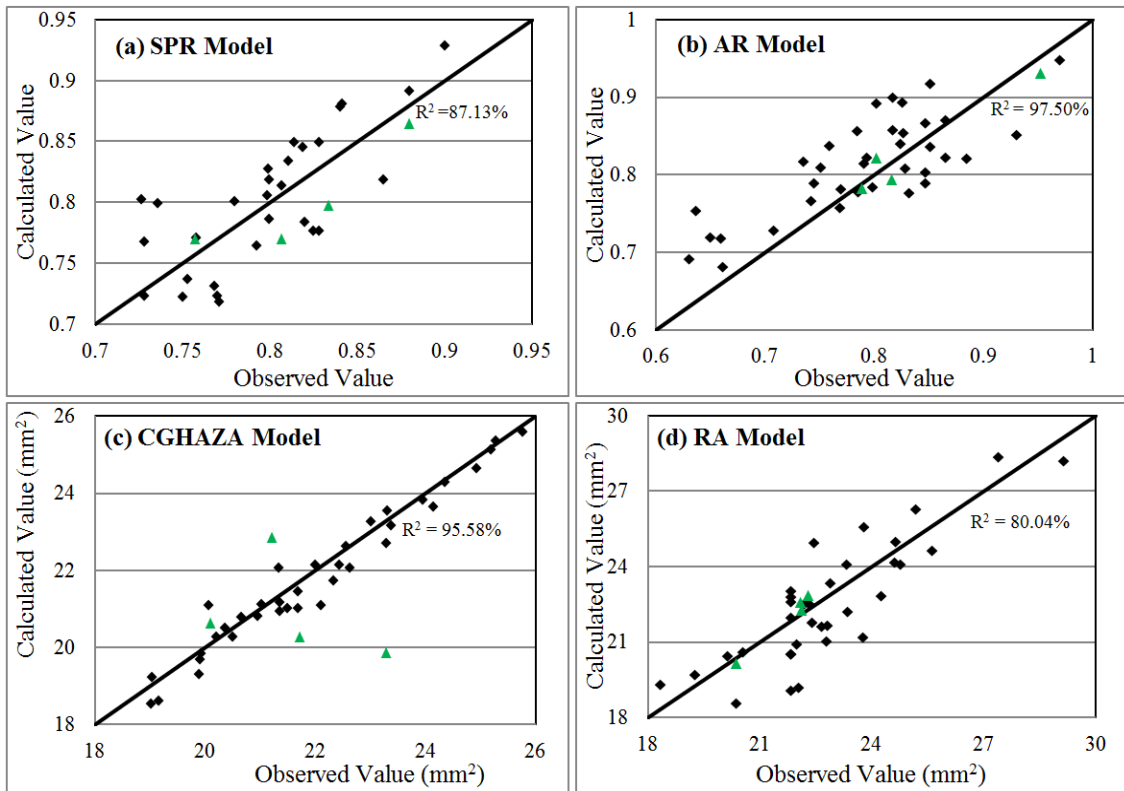


Fig. 5

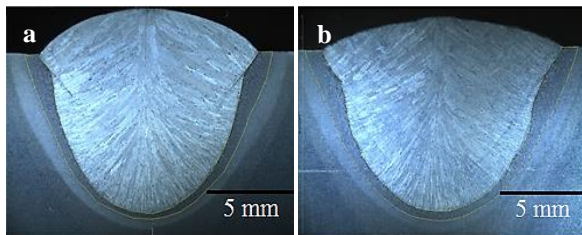
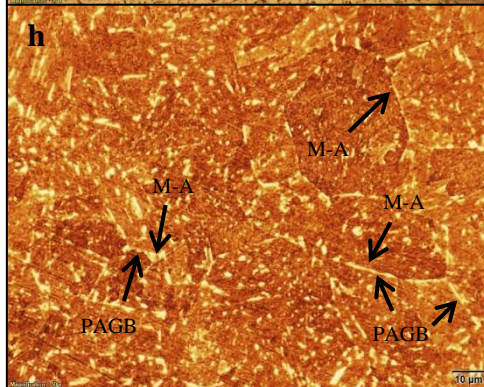
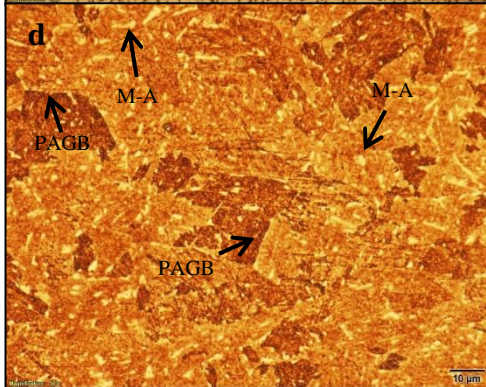
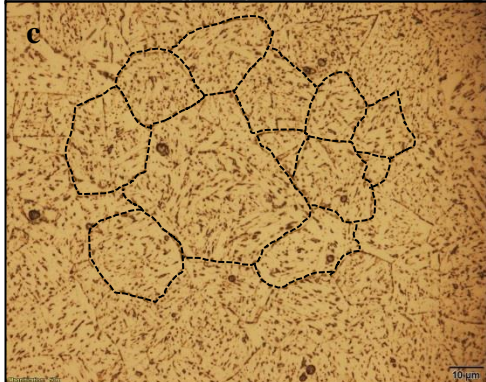
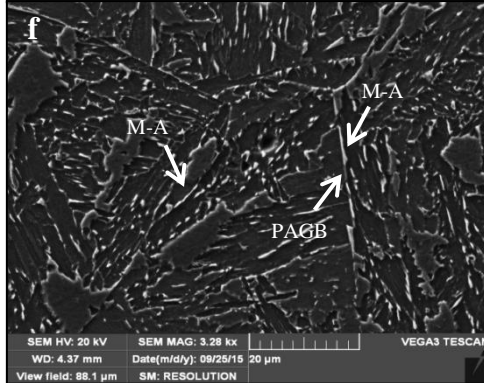
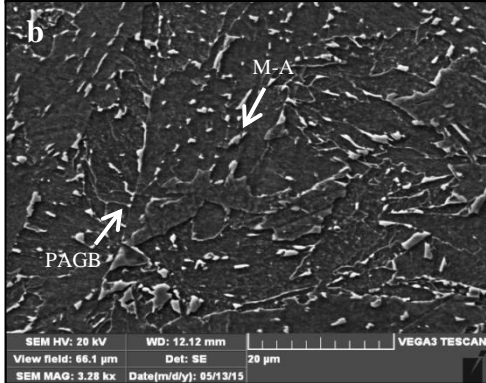
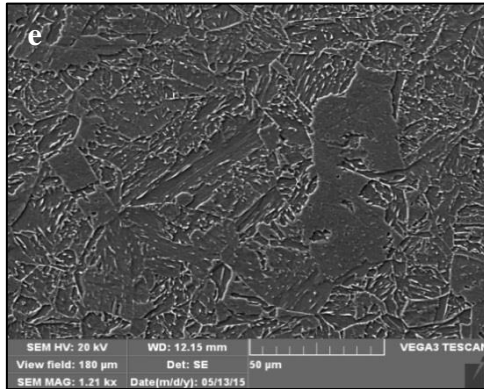
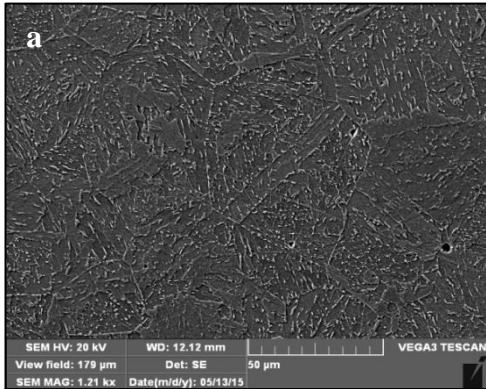


Fig. 6



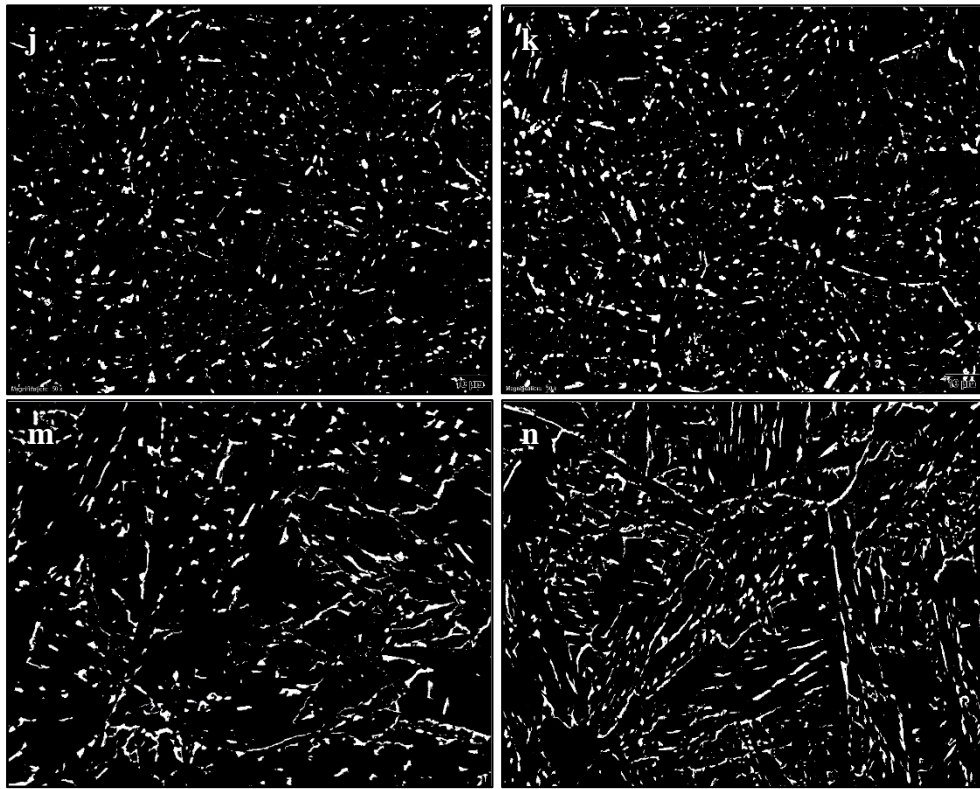


Fig. 7

Table List:

Table 1 X70 microalloyed steel and electrode compositions (wt%)

X70 composition (wt%)									
C	P	S	Mn	Si	N	V+Mo+Nb+Ti	Cu+Ni+Cr+Sn+Al+Ca	Fe	
0.04	0.01	0.001	1.76	0.24	0.01	0.21	0.60	97.13	
Electrode and cold-wire composition (wt%)									
Symbol	C	P	S	Mn	Si	Mo	Ni	Cr	Cu
BA-S2Mo	0.10	0.007	0.01	1.04	0.1	0.56	0.02	0.03	0.03

Table 2 CWTSAW process parameters and levels

<i>Symbol</i>	<i>Process Parameter</i>	<i>Notation</i>	<i>Unit</i>	<i>Level 1</i>	<i>Level 2</i>	<i>Level 3</i>
A	Cold-Wire Position	CWP	Lagging	Side
B	Heat Input-Lead Electrode	HIL	kJ/mm	1.10	1.20
C	Heat Input-Trail Electrode	HIT	kJ/mm	0.95	1.08
D	Voltage-Lead Electrode	VL	V	28	30
E	Voltage-Trail Electrode	VT	V	30	34
F	Travel Speed	TS	mm/s	25.40	26.67	27.94
G	Cold-Wire Angle	CWA	degree	32	47	63
H	Cold-Wire Feed Speed	CWFS	mm/s	8.50	10.60	12.70

Table 3 Design matrix based on L36 orthogonal array (the numbers refer to the parameter levels given in Table 2)

Weld no.	A (CWP)	B (HIL)	C (HIT)	D (VL)	E (VT)	F (TS)	G (CWA)	H (CWFS)
1	1	1	1	1	1	1	1	1
2	1	1	1	1	1	2	2	2
3	1	1	1	1	1	3	3	3
4	1	1	1	1	1	1	1	1
5	1	1	1	1	1	2	2	2
6	1	1	1	1	1	3	3	3
7	1	1	2	2	2	1	1	2
8	1	1	2	2	2	2	2	3
9	1	1	2	2	2	3	3	1
10	1	2	1	2	2	1	1	3
11	1	2	1	2	2	2	2	1
12	1	2	1	2	2	3	3	2
13	1	2	2	1	2	1	2	3
14	1	2	2	1	2	2	3	1
15	1	2	2	1	2	3	1	2
16	1	2	2	2	1	1	2	3
17	1	2	2	2	1	2	3	1
18	1	2	2	2	1	3	1	2
19	2	1	2	2	1	1	2	1
20	2	1	2	2	1	2	3	2
21	2	1	2	2	1	3	1	3
22	2	1	2	1	2	1	2	2
23	2	1	2	1	2	2	3	3
24	2	1	2	1	2	3	1	1
25	2	1	1	2	2	1	3	2
26	2	1	1	2	2	2	1	3
27	2	1	1	2	2	3	2	1
28	2	2	2	1	1	1	3	2
29	2	2	2	1	1	2	1	3
30	2	2	2	1	1	3	2	1
31	2	2	1	2	1	1	3	3
32	2	2	1	2	1	2	1	1
33	2	2	1	2	1	3	2	2
34	2	2	1	1	2	1	3	1
35	2	2	1	1	2	2	1	2
36	2	2	1	1	2	3	2	3

Table 4 Weld Parameters used for CWTSAW and TSAW comparison

Weld type	HIL (kJ/mm)	HIT (kJ/mm)	VL (V)	VT (V)	TS (mm/sec)	CWP	CWA (degrees)	CWFS (mm/sec)
TSAW	1.15	1.00	30	33	25.4	NA	NA	NA
CWTSAW	1.15	1.00	30	33	25.4	Lagging	47	8.5

Table 5 Suitable levels of CWTSAW process parameters

SPR	CWP1	HI-L1	HI-T1	V-L1	V-T1	T.S.3	CWA3	CWFS1
AR	CWP1	HI-L2	HI-T1	V-L1	V-T1	T.S.3	CWA1	CWFS1
CGHAZA	CWP2	HI-L1	HI-T1	V-L2	V-T2	T.S.3	CWA3	CWFS2
RA	CWP1	HI-L1	HI-T1	V-L2	V-T2	T.S.2	CWA1	CWFS1
Dilution	CWP1	HI-L1	HI-T2	V-L2	V-T1	T.S.3	CWA3	CWFS1

Table 6 CWTSAW samples used for confirmatory test of the developed equations

Weld id.	A(CWA)	B(HIL)	C(HIT)	D(VL)	E(VT)	F(TS)	G(CWA)	H(CWFS)
CT17	1	1.153	1.052	30	34	26.67	47	10.6
CT18	2	1.153	1.052	30	34	26.67	47	10.6
CT19	2	1.164	0.95	30	34	29.63	47	10.6
CT20	1	1.199	1.019	30	34	27.52	47	10.6

Table 7 Effect of cold-wire addition on dilution, micro-hardness and geometry characteristics (three weld samples were analyzed for each welding condition)

Heat-input: 2.15 kJ/mm	CWTSAW (CWFS: 8.5 mm/s)	TSAW
<i>CGHAZ area (mm²)</i>	19.10±0.81	21.30±0.63
<i>Reinforcement area (mm²)</i>	24.90±1.82	18.60±1.50
<i>Penetration area (mm²)</i>	86.50±0.50	97.30±1.04
<i>Dilution</i>	0.56±0.01	0.65±0.02
<i>CGHAZ hardness (HV0.5)</i>	222.93±6.46	236.11±7.02

Table A1 Measured weld characteristics- three specimens were characterized for each welding run

Weld no.	SPR	AR	CGHAZA (mm ²)	RA (mm ²)	Dilution	CGHAZ Hardness (HV0.5)	WM Hardness (HV0.5)
1	0.83±0.04	0.90±0.05	22.44±1.38	22.57±0.14	0.60±0.03	234.85±5.01	244.33±1.53
2	0.80±0.04	0.84±0.04	21.34±0.33	22.98±0.45	0.58±0.01	234.33±2.96	243.89±5.22
3	0.82±0.04	0.80±0.04	20.07±1.36	22.74±0.71	0.60±0.02	233.70±8.11	252.50±4.04
4	0.81±0.02	0.86±0.01	22.02±1.36	20.51±3.21	0.59±0.02	232.20±5.16	250.77±4.38
5	0.87±0.01	0.92±0.02	22.62±0.47	19.07±1.28	0.61±0.01	229.33±5.45	239.92±6.73
6	0.83±0.02	0.87±0.04	22.12±1.41	20.51±0.68	0.58±0.01	233.54±7.04	248.09±3.48
7	0.74±0.02	0.69±0.03	25.19±0.23	21.74±1.25	0.60±0.02	231.36±7.80	245.64±3.10
8	0.73±0.01	0.68±0.01	23.95±1.04	22.52±1.62	0.57±0.02	235.31±4.92	250.38±3.50
9	0.90±0.08	0.81±0.10	20.36±0.39	21.59±4.23	0.61±0.03	237.88±6.83	243.11±3.16
10	0.74±0.04	0.86±0.13	21.03±1.36	20.61±0.99	0.58±0.01	236.30±4.08	245.36±4.52
11	0.77±0.02	0.72±0.04	20.22±1.05	20.41±1.46	0.59±0.01	228.00±6.94	242.62±4.46
12	0.89±0.01	0.87±0.00	19.04±0.44	18.54±1.12	0.63±0.01	240.75±9.71	247.71±3.22
13	0.75±0.02	0.82±0.01	25.27±0.81	24.98±0.87	0.57±0.01	227.77±7.40	245.90±9.27
14	0.80±0.02	0.82±0.01	22.57±0.99	23.35±0.80	0.61±0.01	238.29±7.37	253.75±5.38
15	0.80±0.02	0.79±0.04	20.66±0.40	21.15±3.26	0.62±0.02	227.69±5.07	247.70±3.47
16	0.76±0.01	0.75±0.02	23.02±1.07	24.62±2.01	0.61±0.01	225.38±9.43	241.13±5.51
17	0.75±0.05	0.89±0.04	23.31±0.84	24.04±4.01	0.62±0.02	236.80±9.23	247.40±5.15
18	0.80±0.04	0.84±0.04	19.91±0.50	26.28±2.37	0.61±0.01	226.67±8.28	241.69±5.64
19	0.77±0.05	0.81±0.10	20.51±0.18	21.03±4.64	0.61±0.04	224.92±9.62	244.00±5.61
20	0.79±0.07	0.79±0.08	19.89±0.55	22.51±5.05	0.62±0.04	229.38±4.50	236.33±2.12
21	0.85±0.01	0.85±0.04	19.03±0.48	21.95±0.47	0.64±0.01	233.80±4.89	247.42±6.00
22	0.73±0.01	0.73±0.02	21.50±0.19	25.53±1.48	0.58±0.01	226.50±4.19	239.92±5.85
23	0.76±0.01	0.78±0.07	19.93±0.42	22.79±4.04	0.59±0.01	231.00±4.85	237.50±4.74
24	0.81±0.03	0.82±0.01	21.68±0.19	22.17±1.52	0.61±0.01	223.55±6.90	238.92±4.30
25	0.77±0.01	0.72±0.01	21.70±0.41	19.29±2.63	0.58±0.03	227.27±5.08	239.56±3.36
26	0.77±0.02	0.76±0.02	21.38±0.64	14.85±2.56	0.61±0.02	230.33±7.07	240.14±2.85
27	0.79±0.03	0.78±0.05	19.17±0.45	19.69±4.15	0.59±0.03	229.44±6.11	242.18±3.52
28	0.84±0.06	0.89±0.05	25.77±0.92	28.18±2.12	0.59±0.02	223.33±7.00	237.80±1.64
29	0.80±0.05	0.85±0.07	24.14±0.69	29.61±4.31	0.58±0.04	232.56±7.02	239.80±3.58
30	0.87±0.08	0.95±0.10	24.94±0.61	28.31±1.34	0.61±0.02	233.50±9.44	239.38±4.50
31	0.71±0.01	0.78±0.01	21.36±1.10	21.64±0.01	0.59±0.01	232.80±5.16	240.92±2.07
32	0.81±0.03	0.81±0.04	23.30±1.29	19.15±0.61	0.62±0.01	222.57±8.46	238.45±4.87
33	0.80±0.01	0.78±0.01	20.96±0.87	24.92±1.82	0.60±0.01	222.93±6.46	237.55±3.80
34	0.79±0.02	0.84±0.02	24.36±1.11	20.86±0.74	0.61±0.01	226.90±5.01	239.25±3.82
35	0.73±0.01	0.76±0.03	23.38±0.59	24.07±0.76	0.56±0.01	226.42±6.46	240.40±3.85
36	0.79±0.01	0.82±0.02	22.34±0.45	24.16±2.49	0.57±0.02	230.22±6.30	240.43±3.69

Table A2 ANOVA results for seven parametric characteristics

Characteristic		CWP	HIL	HIT	VL	VT	TS	CWA	CWFS	Error
SPR	DF	1	1	1	1	1	2	2	2	3
	Adj SS	0.001	0.001	0.001	0.003	0.007	0.024	0.002	0.006	0.002
	F	0.77	0.65	0.07	1.69	4.57	8.49	0.74	2.27	
	P	0.39	0.43	0.79	0.21	0.04	0.00	0.49	0.10	
AR	DF	1	1	1	1	1	2	2	2	3
	Adj SS	0.001	0.012	0.027	0.105	0.040	0.011	0.050	0.049	0.006
	F	0.03	0.75	1.69	6.61	2.50	0.33	1.57	1.52	
	P	0.86	0.40	0.21	0.01	0.10	0.72	0.23	0.24	
CGHAZA	DF	1	1	1	1	1	2	2	2	3
	Adj SS	0.001	11.872	4.565	15.785	0.256	24.61	1.256	0.350	3.007
	F	0.00	4.57	1.76	6.08	0.10	4.74	0.24	0.07	
	P	0.98	0.04	0.20	0.02	0.76	0.02	0.79	0.94	
RA	DF	1	1	1	1	1	2	2	2	3
	Adj SS	4.338	46.330	86.476	40.443	29.004	2.324	9.253	4.885	12.27
	F	1.26	13.46	25.12	11.75	8.42	0.34	1.34	0.71	
	P	0.27	0.00	0.00	0.00	0.01	0.72	0.28	0.50	
CGHAZ Hardness	DF	1	1	1	1	1	2	2	2	3
	Adj SS	190.51	11.01	1.05	1.05	4.30	33.00	87.93	57.68	16.06
	F	11.69	0.68	0.06	0.06	0.26	1.01	2.70	1.77	
	P	0.01	0.42	0.80	0.80	0.61	0.38	0.08	0.19	
WM Hardness	DF	1	1	1	1	1	2	2	2	3
	Adj SS	355.05	9.50	0.65	2.68	2.90	5.01	14.88	50.86	38.31
	F	29.40	0.80	0.05	0.22	0.24	0.41	0.62	2.10	
	P	0.00	0.38	0.82	0.64	0.63	0.67	0.55	0.10	
Dilution	DF	1	1	1	1	1	2	2	2	3
	Adj SS	0.000	0.000	0.001	0.001	0.001	0.001	0.002	0.002	0.000
	F	0.03	0.00	2.06	4.04	2.32	1.97	2.41	2.37	
	P	0.88	0.97	0.16	0.05	0.14	0.12	0.10	0.10	

Table A3 Mean S/N ratios for CWTSAW process parameters (S/N ratios with higher value are in bold)

Symbol	Parameters	Level	SPR	AR	CGHAZA	RA	Dilution
A	CWP	1	-1.67 ±0.54	-1.09 ±0.58	-26.80±0.70	-26.86 ±0.81	-4.46 ±0.24
		2	-2.11±0.45	-1.23±0.40	-26.80 ±0.77	-27.06±1.44	-4.48±0.28
B	HI-L	1	-2.00 ±0.49	-1.24±0.54	-26.58 ±0.63	-26.53 ±0.99	-4.47 ±0.24
		2	-2.11±0.50	-1.07 ±0.44	-27.02±0.76	-27.39±1.17	-4.48±0.28
C	HI-T	1	-2.02 ±0.49	-1.09 ±0.54	-26.67 ±0.57	-26.35 ±1.06	-4.53±0.25
		2	-2.08±0.51	-1.22±0.45	-26.93±0.85	-27.56±0.92	-4.42 ±0.26
D	V-L	1	-1.96 ±0.43	-0.93 ±0.38	-27.07±0.65	-27.37±1.04	-4.55±0.24
		2	-2.15±0.55	-1.39±0.50	-26.54 ±0.71	-26.54 ±1.13	-4.40 ±0.26
E	V-T	1	-1.91 ±0.45	-1.00 ±0.46	-26.84±0.72	-27.30±1.13	-4.42 ±0.22
		2	-2.19±0.51	-1.32±0.49	-26.77 ±0.75	-26.62 ±1.10	-4.53±0.28
F	TS	1	-2.30±0.46	-1.17±0.65	-27.15±0.68	-27.04±0.97	-4.55±0.19
		2	-2.18±0.43	-1.22±0.46	-26.90±0.59	-26.78 ±1.40	-4.50±0.28
		3	-1.67 ±0.37	1.09 ±0.38	-26.36 ±0.69	-27.05±1.05	-4.37 ±0.28
G	CWA	1	-2.07±0.43	-1.02 ±0.46	-26.83±0.67	-26.76 ±1.40	-4.43±0.30
		2	-2.13±0.48	-1.26±0.50	-26.88±0.70	-27.25±0.99	-4.59±0.22
		3	-1.95 ±0.59	-1.20±0.53	-26.70 ±0.76	-26.87±0.90	-4.40 ±0.23
H	CWFS	1	-1.90 ±0.42	-1.09 ±0.53	-26.85±0.66	-26.79 ±0.87	-4.37 ±0.17
		2	-2.02±0.55	-1.24±0.46	-26.75 ±0.77	-27.11±1.12	-4.48±0.28
		3	-2.23±0.48	-1.14±0.53	-26.81±0.71	-26.98±1.35	-4.57±0.29